Chapter 4

On the evolution of acceleration discontinuities in van der Waals dusty magnetogasdynamics *

"Measure what is measurable,
and make measurable what is not so."

–Galileo Galilei

4.1 Introduction

This chapter presents the study of the evolutionary behavior of plane and cylindrically symmetric acceleration discontinuities along the characteristic path under

* "The contents of this chapter have been published in ***Zeitschrift für Naturforschung A (De Gruyter), Volume 76, 2021."***

the effect of dust particles in a non-ideal magnetogasdynamic flow. The study of acceleration discontinuities received considerable attention because they represent a particular type of non-linear waves, which can be studied by some analytical methods. The process of shock propagation and decay in the characteristic plane is one of the most critical aspect of the acceleration wave theory in gas dynamics. The problem of the study of flow pattern of acceleration discontinuities in different material medium has gained significant attention over recent years due to their application in numerous fields like astrophysics, plasma physics, nuclear science, engineering sciences and space science. Shock waves arise in many supersonic astrophysical flows with an internal angular velocity, causing that flow to become subsonic. This is because the distorted centrifugal potential barrier experienced by such flows can be strong enough to break the motion, and the static solution can only be represented by the shock. Also, shock waves generated by supernova explosions are used to study the theory of self-propagating star formation. As a supernova shock wave enters a gas cloud, it compresses the atmosphere to induce star formation. Some of them are big enough to produce their supernova explosion to keep the cycle going. Arora and Sharma [117] have used the perturbation technique to examine the convergence of strong shock waves in a non-ideal gas and find the global solution to the implosion problem. Singh et al. [118] determined the exact solution of weak shock wave problem with density varying as the power of the distance and examined the behavior of energy for different values of the Mach number. Vishwakarma and Nath [119], Singh et al.[120] have used the similarity method to examine the shock wave propagation under the influence of gravitation. Siddiqui et al. [121] has examined the shock wave propagation for point explosion under the influence of transverse magnetic field.

Acceleration discontinuities or acceleration waves are the discontinuities that occur in the derivative of the solution along the characteristics however, the solution itself remains continuous. Several researchers have generalized the theory of acceleration

waves in various material media, such as ideal gas dynamics, magnetogasdynamics and established the conditions for shock formation and its distortion in the medium. Green [92] have studied the propagation of acceleration discontinuities in elastic material and proved that these discontinuities either becomes shock wave after a finite time or decays eventually. Varley [122] further analyzed the strength of the acceleration fronts in viscoelastic material. Ram [55], Chaturvedi et al.[86] has examined the flow patterns of acceleration waves in magnetogasdynamic flow under the influence of radiation. Singh et al. [62] have further examined the decay and formation of discontinuous wave in non-ideal magnetogasdynamic flow under the effect of radiative heat transfer. Also, Chou et al. [123], Sharma et al. [53], Van et al. [124], Shankar [56], Wu et al. [125] and Keller [126] studied the several differential effects of the weak discontinuity and obtained the conditions for examining the evolutionary process of the weak discontinuity.

Over the past few decades, much attention has been paid to study the dusty gases because of its wide applications to lunar ash burst, nozzle flow, underground explosions, volcanic explosions, bomb blast, supersonic flight in the dusty air, description of star formation and many other physical problems [127, 128, 114, 129, 14, 63, 130, 131]. In all the previous works, no one has analyzed the study of the propagation of acceleration discontinuity in the mixture of van der Waals gas with dust particles under the influence of a magnetic field. In contrast, the study of dusty gases in magnetogasdynamics has broader applications in astrophysics and space science, planetary systems and many other engineering problems [132, 133, 134, 135]. In space science, a few examinations have been done; for example, Eswaraiah et al. [136] have discussed dust properties of starless cloud in the magnetic field geometry. Fanciullo et al. [137] have studied the interplay of dust alignment, grain growth, and magnetic fields in polarization and analyzed the dust evolution to explain polarization in molecular clouds

Dusty gases are the mixture that consists of a gas containing small dust particles. In this mixture, the volume of the particles does not occupy more than 5 % of the mixture's total volume. Many researchers worked in gas dynamics, where they examined the dust particle's effect on the strength of the propagating waves in the various medium of flow. Miura [14, 63] have examined the wave propagation and its behavior through dusty gas layer. Also, he described the condition for the separation of pure gas from a mixture of gas with dust particles. Elperin et al. [138] studied the head-on collision of normal shock waves in the dusty medium numerically and found that the reflected shock waves propagate more gradually in the dusty gas. The authors Chadha et al. [139] and Sahu [140] have discussed the shock wave propagation in non-ideal dusty gas. Higashino [114] have studied the blast wave problem in a dusty medium and discussed that as to how the decay of blast waves is affected in dusty gas. Steiner and Hirschler [141], Pai et al. [64], Chaturvedi et al. [87, 91], Srivastava et al. [101] have examined the evolutionary process of shock waves in dusty gas. Mehla et al. [142] have further discussed the wave propagation in relaxing gases with solid particles.

This work aims to generalize the theory of acceleration waves and to determine the various parameter effects on the flow patterns of the solution curves and examine the possibilities of shock formation and its decay under the action of the magnetic field. The complete outline of this article is summarized into sections as: in section 4.2, we derive the governing equation for magnetogasdynamic flow and determine the characteristic curves that represent the propagation of the waves. In the next section, we introduce characteristic variables and change the fundamental equations in terms of new variables. Section 4.4 contains the derivation of the transport equation which leads to investigate the process of shock formation. The behavior of the solution obtained in the previous section is discussed in the fifth section of this

chapter. The sixth section refers to the interpretation of various parameter effects on the shock formation process and its deformation. The last section concludes all the work in this chapter.

4.2 Basic Equations and its characteristics

The governing system of PDEs describing inviscid planar ($m = 0$) and cylindrically symmetric ($m = 1$) flow of non-ideal magnetogasdynamics with dust particles can be written as [121, 101]

$$\begin{cases} \rho_t + u\rho_x + \rho u_x + m\rho u x^{-1} = 0, \\ \rho\left(u_t + uu_x\right) + p_x + h_x = 0, \\ E_t + uE_x - p\rho^{-2}\left(\rho_t + u\rho_x\right) = 0, \\ h_t + uh_x + 2hu_x + 2hmux^{-1} = 0, \end{cases} \tag{4.1}$$

where ρ denotes the density, p is the pressure, t is the time and u represents the velocity in $x-$direction. The magnetic pressure h is defined as $h = \frac{\sigma H^2}{2}$, where H and σ denote transverse magnetic field and the magnetic permeability, respectively. The parameter E is the internal energy per unit mass of the mixture defined as

$$E = \frac{(1 - Z)(1 - \tilde{b}\rho)p}{(\Gamma - 1)\rho}, \tag{4.2}$$

where $Z = V_{sp}/V_g$ denotes the volume fraction of the dust particles. The volume of the dust particles is denoted by V_{sp} and V_g denotes the entire volume of the mixture; $\tilde{b} = b(1 - k_p)$ where b is the parameter of non-idealness. The Grüneisen coefficient Γ is given by

$$\Gamma = \frac{\gamma(1+\lambda\beta)}{(1+\lambda\beta\gamma)},$$

where $\lambda = k_p/(1-k_p)$, $\gamma = c_p/c_v$, $\beta = c_{sp}/c_p$. The parameter c_{sp} is the specific heat of dust particles, c_p and c_v represent the specific heat of the gas at constant pressure and constant volume, respectively. Here $k_p = m_{sp}/m_g$ is known as the mass fraction of the solid particles, where m_{sp} is the mass of the solid particles and and m_g denotes the total mass of the mixture. Z and k_p are related by $Z = \theta\rho$, $\theta = k_p/\rho_{sp}$, where ρ_{sp} is the specific density of the dust particles.

The equation of state of the mixture of the non-ideal gas and small solid particles is given as [101]

$$p = \frac{(1-k_p)}{(1-Z)(1-\tilde{b}\rho)}\rho RT, \tag{4.3}$$

where R denotes the gas constant and T is the temperature.

By using equations (4.2) and (4.3), (4.1) can be written as

$$\begin{cases} \rho_t + u\rho_x + \rho u_x + m\rho u x^{-1} = 0, \\ \rho\left(u_t + uu_x\right) + p_x + h_x = 0, \\ p_t + up_x - a^2\left(\rho_t + u\rho_x\right) = 0, \\ h_t + uh_x - e^2\left(\rho_t + u\rho_x\right) = 0, \end{cases} \tag{4.4}$$

where $e = (\frac{2h}{\rho})^{\frac{1}{2}}$ is Alfvén speed and a is the speed of sound in non-ideal gas with dust particles defined as

$$a^2 = \frac{(\Gamma - \omega_2\rho^2)p}{(1-\omega_1\rho+\omega_2\rho^2)\rho},$$

where $\omega_1 = \theta + \tilde{b}$ and $\omega_2 = \theta\tilde{b}$.

The following cases arise, depending on the values of the parameters θ and b.

Case 1: When $\theta = 0$ and $b \neq 0$, then Γ becomes γ, $a^2 = \frac{\gamma p}{(1-b\rho)\rho}$, i.e. the flow

becomes van der Waals gas flow in a dust free medium.

Case 2: When $\theta = 0$ and $b = 0$, then Γ becomes γ, $a^2 = \frac{\gamma p}{\rho}$, and the mixture becomes ideal in the absence of dust particles.

Case 3: When $\theta \neq 0$ and $b = 0$, in this case $\Gamma \neq 0$, $a^2 = \frac{\Gamma p}{(1-Z)\rho}$, and the flow becomes ideal gas flow with dust particles.

Case 4: When $\theta \neq 0$ and $b \neq 0$, in this case $\Gamma \neq 0$, $a^2 = \frac{(\Gamma - \omega_2\rho^2)p}{(1-\omega_1\rho+\omega_2\rho^2)\rho}$, and the flow becomes non-ideal gas flow with dust particles.

The matrix form of (4.4) can be written as

$$U_t + AU_x + B = 0. \tag{4.5}$$

Here U, B are the column vectors and A is a square matrix given below

$$U = \begin{pmatrix} \rho \\ u \\ p \\ h \end{pmatrix}, \quad B = \begin{pmatrix} \frac{m\rho u}{x} \\ 0 \\ \frac{m\rho a^2 u}{x} \\ \frac{2muh}{x} \end{pmatrix} \text{ and } A = \begin{pmatrix} u & \rho & 0 & 0 \\ 0 & u & \rho^{-1} & \rho^{-1} \\ 0 & \rho a^2 & u & 0 \\ 0 & \rho e^2 & 0 & u \end{pmatrix},$$

where $U(x,t)$ is a continuous function which satisfy equation (4.5) everywhere in the characteristic plane except at the characteristic curve $S(t)$. Across the characteristic curve $S(t)$, U remains continuous, but the derivatives U_x and U_t are discontinuous. Now, along the characteristic curve $S(t)$, we have

$$\frac{\partial}{\partial t}[U] = [U_t] + \frac{dS(t)}{dt}[U_x], \tag{4.6}$$

where $\dfrac{\partial}{\partial t}$ denotes the partial derivative with respect to time t.

Since U is a continuous function, therefore $[U] = 0$. Taking jump in (4.5) and using

equation (4.6) with above condition $[U] = 0$, we obtain

$$\left(A - \frac{dS(t)}{dt} I\right) [U_x] = 0, \tag{4.7}$$

where I denotes the identity matrix of order 4×4. From equation (4.7), we observe that along the characteristic curve, $\frac{dS}{dt}$ is an eigenvalue of the matrix A. There are four families of characteristic curves corresponding to the system (4.5), two of which are given by

$$\frac{dx}{dt} = u \pm C, \tag{4.8}$$

where the characteristic curve $u + C$ represents the wave propagation in the positive x-direction, and $u - C$ represents the wave propagation in negative x-direction with magnetosonic speed C defined as $C = (a^2 + e^2)^{\frac{1}{2}}$. The other two of the characteristic curves

$$\frac{dx}{dt} = u, u, \tag{4.9}$$

represent the particle path.

4.3 Acceleration discontinuities in characteristic plane

We define two characteristic variables ζ and ψ, where ζ is the particle tag and ψ is the wave tag such that ζ is constant along the particle path $\frac{dx}{dt} = u$, and the wave tag ψ is constant along the characteristic $\frac{dx}{dt} = u + C$. Therefore, if the characteristic wavefront moves through a particle at time t^*, then the particle tag ζ can be marked

as $\zeta = t^*$, and if the piston generates outgoing wave at time $t^{'}$, then we can label the wave tag ψ as $\psi = t^{'}$.

Hence, corresponding to each pair (ψ, ζ), we can find a pair (x, t) such that $x = x(\psi, \zeta)$, $t = t(\psi, \zeta)$. Now, the characteristic variables ψ and ζ satisfy the following conditions

$$x_\psi = ut_\psi, \qquad x_\zeta = (u + C)t_\zeta. \tag{4.10}$$

Under the above transformation (4.10), U_t and U_x are transformed into the following form

$$U_t = \frac{U_\zeta x_\psi - U_\psi x_\zeta}{J}, \qquad U_x = \frac{U_\psi t_\zeta - U_\zeta t_\psi}{J}, \tag{4.11}$$

where $J = \dfrac{\partial(x,t)}{\partial(\psi,\zeta)} = -Ct_\psi t_\zeta$, is the Jacobian of transformation.

By using equation (4.11), equation (4.4) can be written as

$$C\rho_\psi t_\zeta - \rho\left(u_\psi t_\zeta - u_\zeta t_\psi - \frac{muCt_\psi t_\zeta}{x}\right) = 0, \tag{4.12}$$

$$\rho C u_\psi t_\zeta - p_\psi t_\zeta + p_\zeta t_\psi - h_\psi t_\zeta + h_\zeta t_\psi = 0, \tag{4.13}$$

$$Cp_\psi t_\zeta - \rho a^2\left(u_\psi t_\zeta - u_\zeta t_\psi - \frac{muCt_\psi t_\zeta}{x}\right) = 0, \tag{4.14}$$

$$Ch_\psi t_\zeta - 2h(u_\psi t_\zeta - u_\zeta t_\psi) + \frac{2mhuct_\psi t_\zeta}{x} = 0. \tag{4.15}$$

Using eqs. (4.13) $-$ (4.15) in (4.12), we obtain

$$p_\zeta + \rho C u_\zeta + h_\zeta + \frac{m\rho C^2 u t_\zeta}{x} = 0, \tag{4.16}$$

The sub-scripts ψ and ζ represents the partial derivative with respect to ψ and ζ, respectively.

The boundary conditions at the wave front at $\psi = 0$ are

$$[p] = 0, \;\; [\rho] = 0, \;\; [u] = 0, \;\; [h] = 0, \;\; t = \zeta. \tag{4.17}$$

It is given that the flow ahead of the wave is uniform and at rest, therefore we have

$$\rho_\zeta = 0, \; p_\zeta = 0, \; u_\zeta = 0, \; h_\zeta = 0 \;\text{ and }\; t_\zeta = 1 \quad \text{ at } \; \psi = 0. \tag{4.18}$$

Using (4.17) and (4.18) in (4.15) , (4.13) and (4.10) and evaluating at $\psi = 0$, we have

$$h_\psi = \left(\frac{2h_0}{C_0}\right) u_\psi, \tag{4.19}$$

$$p_\psi = \rho_0 C_0 u_\psi - \left(\frac{2h_0}{C_0}\right) u_\psi, \tag{4.20}$$

$$x_\psi = 0, \quad x_\zeta = C_0. \tag{4.21}$$

Here, the subscript '0'denotes the value of flow variables evaluated at the front of the shock. Using (4.18) in (4.11), yields

$$\left[\frac{\partial u}{\partial x}\right] = Y = -\frac{u_\psi}{C_0 t_\psi}, \quad \text{ at } \; \psi = 0, \tag{4.22}$$

where Y denote the amplitude of the wave at $\psi = 0$.

4.4 Amplitude of the disturbance

Now, we use the results established in sections 4.2 and 4.3 to determine the conditions under which shock will form. By taking derivative of equation (4.10), (4.16) and

(4.20) with respect to ψ and ζ, at $\psi = 0$, we get

$$\frac{u_{\psi\zeta}}{t_\psi} = \frac{mC_0}{2\zeta}Y, \tag{4.23}$$

$$\frac{t_{\psi\zeta}}{t_\psi} = \left\{\frac{3}{2} - \frac{1}{2\epsilon}\left(\frac{3\Gamma - \omega_2\rho_0^2}{\Gamma - \omega_2\rho_0^2} - \frac{\Gamma + 1 - 2\omega_2\rho_0^2}{1 - \omega_1\rho_0 + \omega_2\rho_0^2}\right)\right\}Y, \tag{4.24}$$

where $\epsilon = \left(1 + \frac{e_0^2}{a_0^2}\right)$.

Differentiating equation (4.22) with respect to ζ and using equations (4.23) and (4.24), yields

$$\frac{dY}{d\zeta} + \frac{m}{2\zeta}Y + \left\{\frac{3}{2} - \frac{1}{2\epsilon}\left(\frac{3\Gamma-\omega_2\rho_0^2}{\Gamma-\omega_2\rho_0^2} - \frac{\Gamma+1-2\omega_2\rho_0^2}{1-\omega_1\rho_0+\omega_2\rho_0^2}\right)\right\}Y^2 = 0, \tag{4.25}$$

at $\psi = 0$.

Now, we introduce non-dimensional quantities given as

$$\eta = \frac{Y}{Y^*}, \quad \mu = \frac{\zeta - \zeta^*}{2\zeta^*} \text{ and } \delta = Y^*\zeta^*, \tag{4.26}$$

where η, δ and μ are the wave amplitude, initial acceleration and time respectively. The superscript '*' has been used to indicate the value of the parameters at $t = t^*$. With the help of (4.26), equation (4.25) can be written in the dimensionless form as

$$\frac{d\eta}{d\mu} + \frac{m}{2\mu + 1}\eta + \left\{3 - \frac{1}{\epsilon}\left(\frac{3\Gamma - \omega_2\rho_0^2}{\Gamma - \omega_2\rho_0^2} - \frac{\Gamma + 1 - 2\omega_2\rho_0^2}{1 - \omega_1\rho_0 + \omega_2\rho_0^2}\right)\right\}\delta\eta^2 = 0, \tag{4.27}$$

at $\psi = 0$.

Equation (4.27) is a Bernoulli type differential equation with η as a dependent variable and μ is an independent variable. The solution of (4.27) is given as

$$\eta = \left\{(2\mu+1)^{\frac{m}{2}}\left(1 + \left(3 - \frac{1}{\epsilon}\left(\frac{3\Gamma-\omega_2\rho_0^2}{\Gamma-\omega_2\rho_0^2} - \frac{\Gamma+1-2\omega_2\rho_0^2}{1-\omega_1\rho_0+\omega_2\rho_0^2}\right)\right)\frac{\delta(2\mu+1)^{1-\frac{m}{2}}}{2(1-\frac{m}{2})}\right)\right\}^{-1}. \tag{4.28}$$

From equations (4.22) and (4.28), we obtained that for the shock formation we must have $t_\psi = 0$, i.e.

$$1+\left(3-\frac{1}{\epsilon}\left(\frac{3\Gamma-\omega_2\rho_0^2}{\Gamma-\omega_2\rho_0^2}-\frac{\Gamma+1-2\omega_2\rho_0^2}{1-\omega_1\rho_0+\omega_2\rho_0^2}\right)\right)\frac{\delta(2\mu+1)^{1-\frac{m}{2}}}{2(1-\frac{m}{2})}=0. \tag{4.29}$$

Equation (4.29) indicates that the compressive discontinuities ($\delta < 0$) end with the shock wave.

4.5 Behavior of Acceleration discontinuities

In this section, we investigate the nature of the solution obtained in the previous section for both planar ($m = 0$) and cylindrically symmetric ($m = 1$) case and discuss the possibilities of formation and distortion of the shock. Consider the following cases to analyze the behavior of the propagating waves under the effect of various parameters.

Case I. Planar flow (m=0):

By substituting $m = 0$ in (4.28), we get

$$\eta=\left\{1+\left(3-\frac{1}{\epsilon}\left(\frac{3\Gamma-\omega_2\rho_0^2}{\Gamma-\omega_2\rho_0^2}-\frac{\Gamma+1-2\omega_2\rho_0^2}{1-\omega_1\rho_0+\omega_2\rho_0^2}\right)\right)\frac{\delta(2\mu+1)}{2}\right\}^{-1}. \tag{4.30}$$

Using equation (4.30) in (4.26), we have

$$Y=\frac{Y^*}{\left\{1+\left(3-\frac{1}{\epsilon}\left(\frac{3\Gamma-\omega_2\rho_0^2}{\Gamma-\omega_2\rho_0^2}-\frac{\Gamma+1-2\omega_2\rho_0^2}{1-\omega_1\rho_0+\omega_2\rho_0^2}\right)\right)\frac{\delta(2\mu+1)}{2}\right\}}. \tag{4.31}$$

From equation (4.31), it can be seen that the amplitude of expansive discontinuities ($\delta > 0$) decays and eventually vanishes. Also, the solution curves representing (4.31) shows that the decay time for the expansive discontinuities is increased due

to an added effect of mass fraction of the dust particles for both magnetic and non-magnetic case.

Case II. Cylindrically symmetric flow (m=1):

For cylindrically symmetric flow,

$$\eta = \left\{(2\mu+1)^{\frac{1}{2}}\left(1+\left(3-\frac{1}{\epsilon}\left(\frac{3\Gamma-\omega_2\rho_0^2}{\Gamma-\omega_2\rho_0^2}-\frac{\Gamma+1-2\omega_2\rho_0^2}{1-\omega_1\rho_0+\omega_2\rho_0^2}\right)\right)\delta(2\mu+1)^{\frac{1}{2}}\right)\right\}^{-1}. \quad (4.32)$$

Using equation (4.32) in (4.26), the solution of (4.27) is

$$Y = \frac{Y^*}{\left\{(2\mu+1)^{\frac{1}{2}}\left(1+\left(3-\frac{1}{\epsilon}\left(\frac{3\Gamma-\omega_2\rho_0^2}{\Gamma-\omega_2\rho_0^2}-\frac{\Gamma+1-2\omega_2\rho_0^2}{1-\omega_1\rho_0+\omega_2\rho_0^2}\right)\right)\delta(2\mu+1)^{\frac{1}{2}}\right)\right\}}. \quad (4.33)$$

Equation (4.33) shows the flattening of expansive discontinuities in cylindrically symmetric flow has a similar trend as in the case of planar flow.

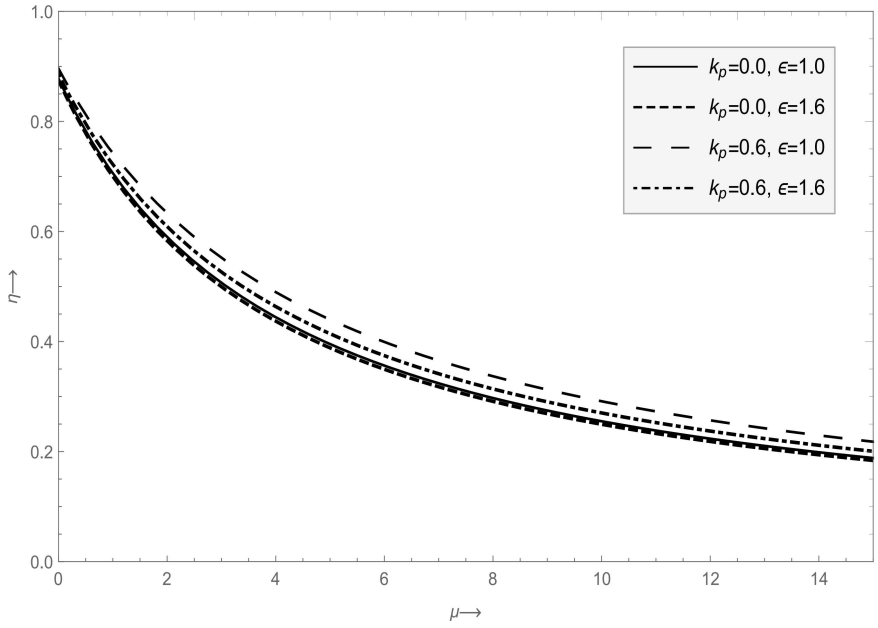

FIGURE 4.1: Flow patterns of the expansive discontinuities with $\gamma = 1.67$, $b = 0.0$, $\beta = 0.8$ and $\delta = 0.1$ for planar symmetry.

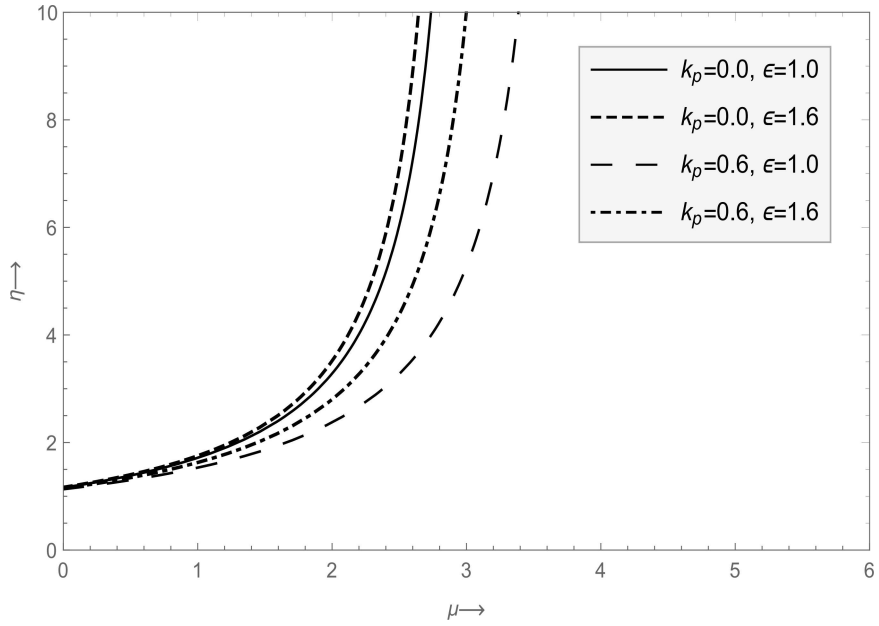

FIGURE 4.2: Flow patterns of the compressive discontinuities with $\gamma = 1.67$, $b = 0.0$, $\beta = 0.8$ and $\delta = -0.1$ for planar symmetry.

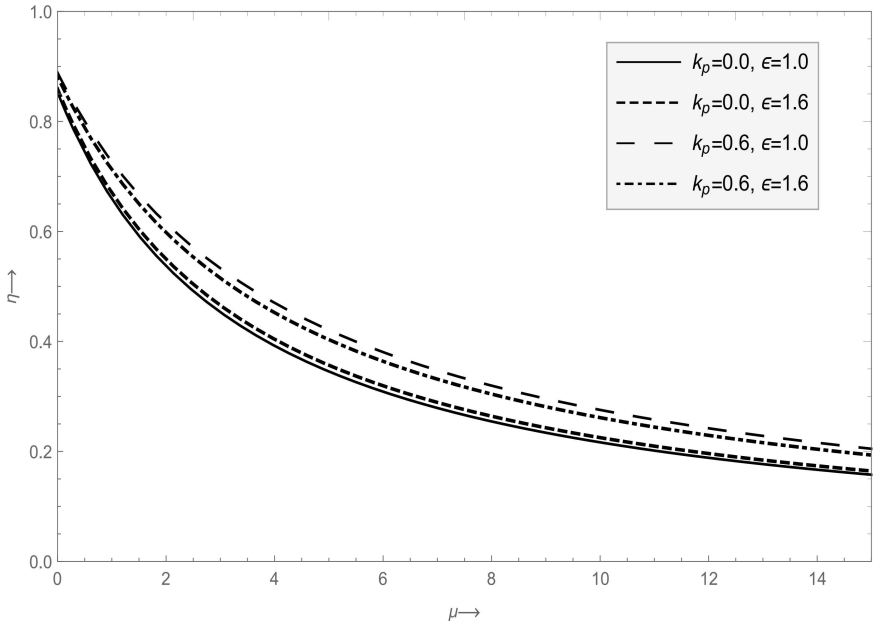

FIGURE 4.3: Flow patterns of the expansive discontinuities with $\gamma = 1.67$, $b = 0.2$, $\beta = 0.8$ and $\delta = 0.1$ for planar symmetry.

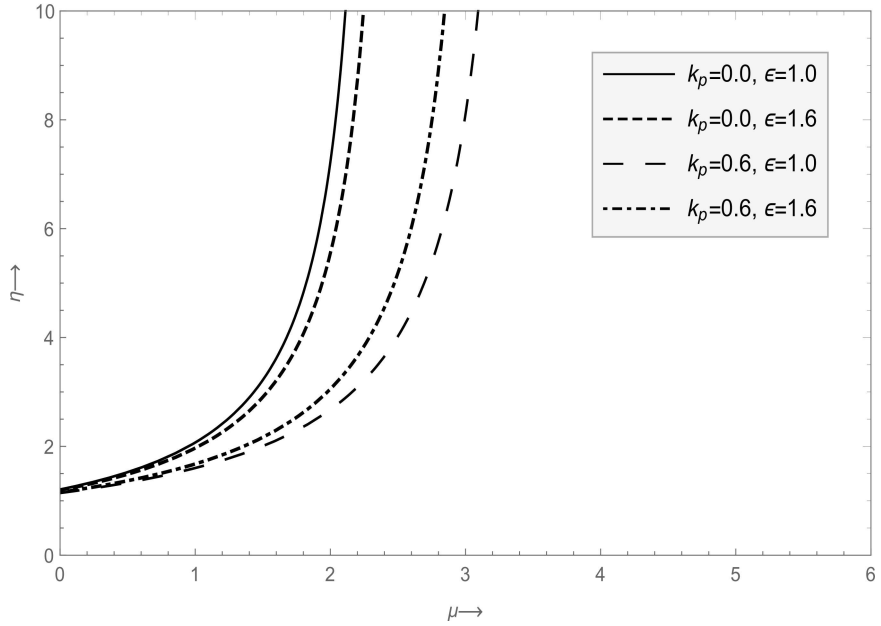

FIGURE 4.4: Flow patterns of the compressive discontinuities with $\gamma = 1.67$, $b = 0.2$, $\beta = 0.8$ and $\delta = -0.1$ for planar symmetry.

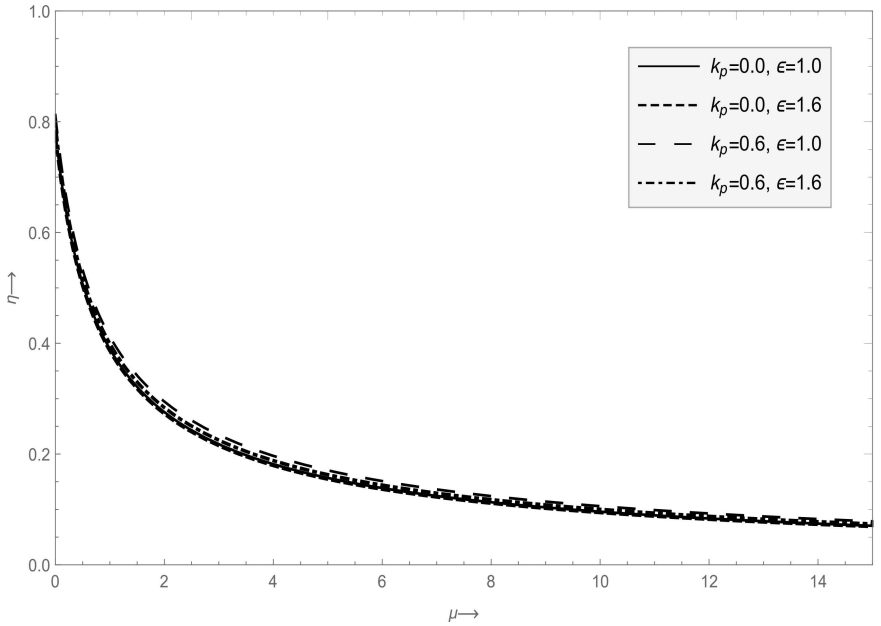

FIGURE 4.5: Flow patterns of the expansive discontinuities with $\gamma = 1.67$, $b = 0.0$, $\beta = 0.8$ and $\delta = 0.1$ for cylindrical symmetry ($m = 1$).

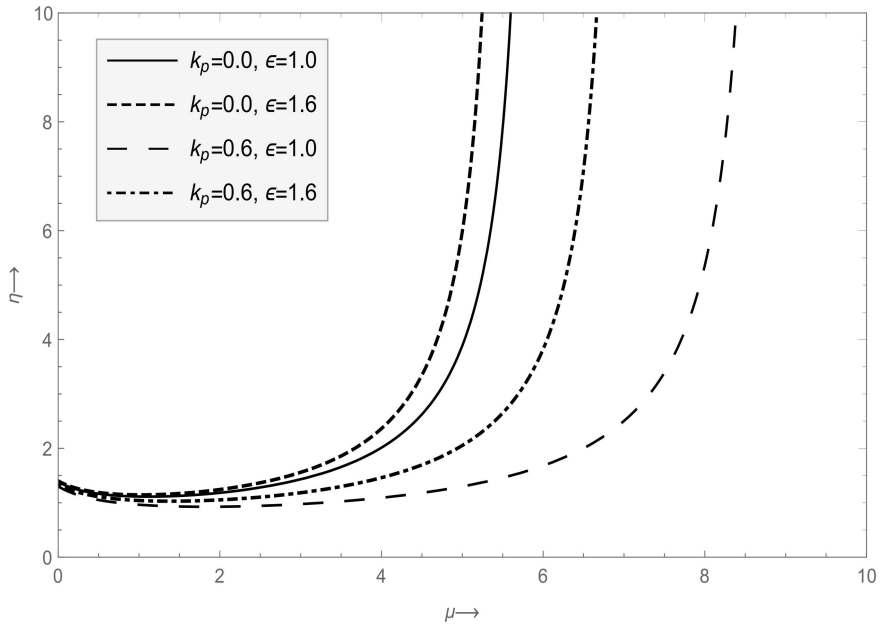

FIGURE 4.6: Flow patterns of the compressive discontinuities with $\gamma = 1.67$, $b = 0.0$, $\beta = 0.8$ and $\delta = -0.1$ for cylindrical symmetry ($m = 1$).

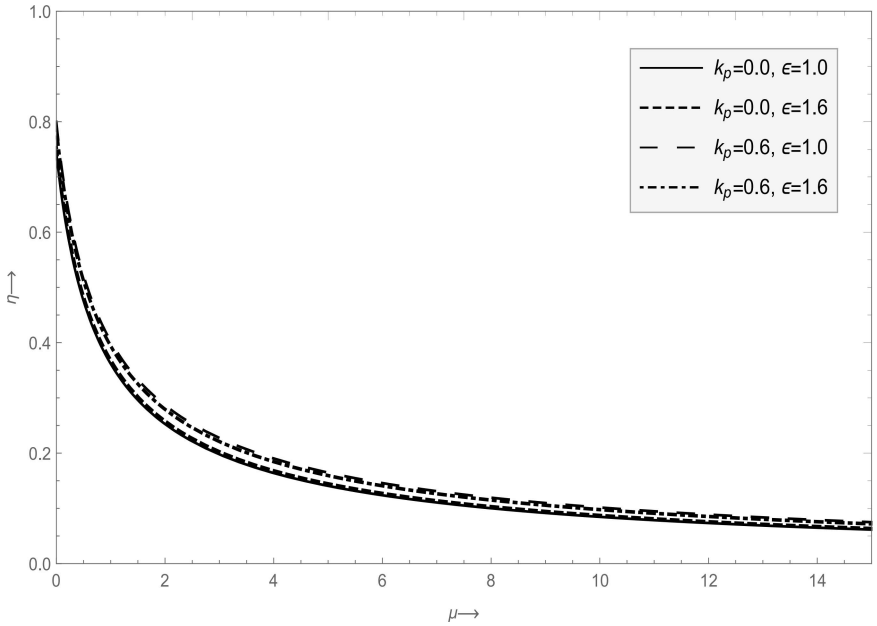

FIGURE 4.7: Flow patterns of the expansive discontinuities with $\gamma = 1.67$, $b = 0.2$, $\beta = 0.8$ and $\delta = 0.1$ for cylindrical symmetry ($m = 1$).

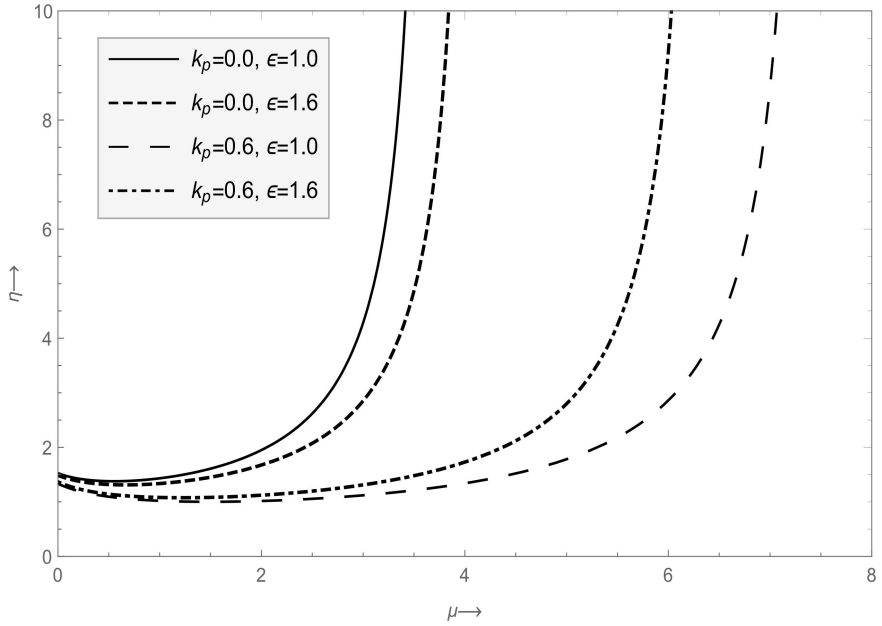

FIGURE 4.8: Flow patterns of the compressive discontinuities with $\gamma = 1.67$, $b = 0.2$, $\beta = 0.8$ and $\delta = -0.1$ for cylindrical symmetry ($m = 1$).

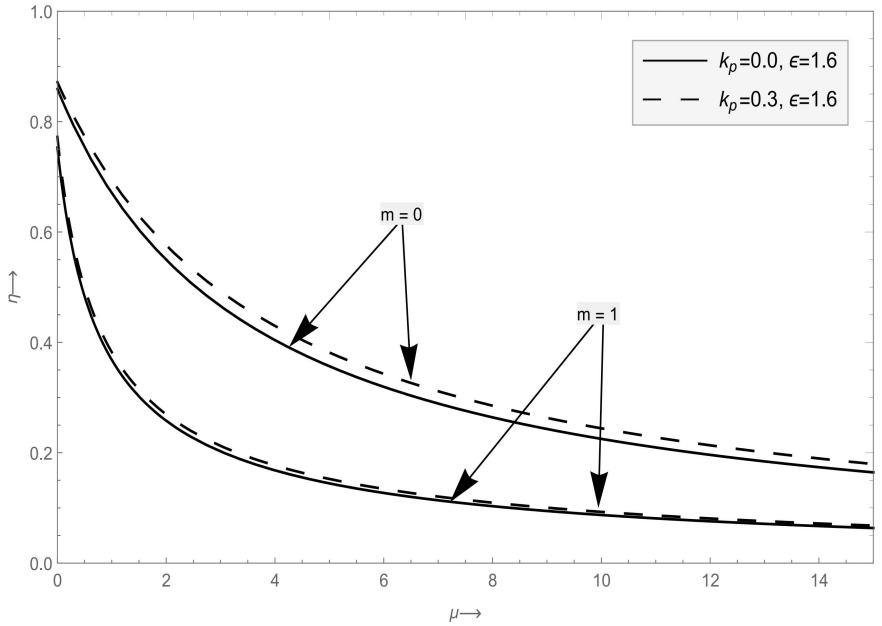

FIGURE 4.9: Flow patterns of the expansive discontinuities for planar($m = 0$) and cylindrically symmetric ($m = 1$) dusty gas flow with $b = 0.2$.

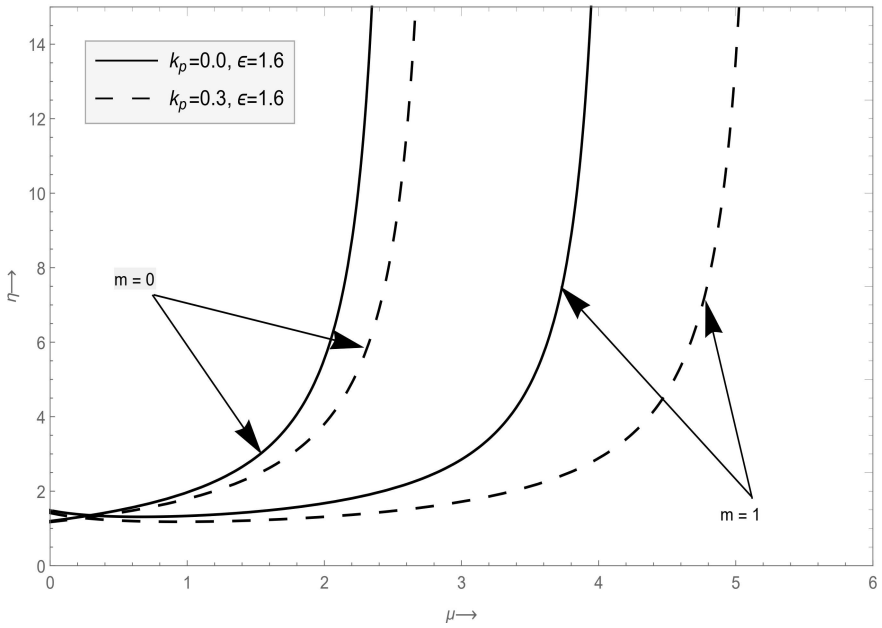

FIGURE 4.10: Flow patterns of the compressive discontinuities for planar($m = 0$) and cylindrically symmetric ($m = 1$) dusty gas flow with $b = 0.2$.

4.6 Results and Discussion

We discuss the consequences of the complete analysis of the preceding sections and investigate the flow patterns in each case for appropriate values of the parameters governing the dusty magnetogasdynamic flow. We investigate the growth and decay behavior of shock for magnetic and non-magnetic case in characteristic plane . Also, we discuss how the van der Waals excluded volume b and the mass fraction k_p influences the shock formation for both planar and cylindrically symmetric flows.

The solution curves presented in Fig.4.1 shows the decay process for $\delta > 0$ in planar ideal dusty gas flow for magnetic and non-magnetic case. Here $\epsilon = 1$ corresponds to the non-magnetic case and $\epsilon = 1.6$ corresponds to the magnetic case, $\delta > 0$ represents the expansive discontinuities and $\delta < 0$ represents the compressive discontinuities. It is found that the presence of mass fraction k_p together with ϵ reduces the rate

of decay for $\delta > 0$. Also, we can see that the parameter ϵ in the absence of dust particles accelerates the decay of propagating waves for $\delta > 0$. Thus, the mass fraction k_p has reverse effect in comparison with the parameter ϵ on the flattening of the expansive discontinuities ($\delta > 0$). The solution curves presented in Fig.4.2 shows the growth process for $\delta < 0$ in planar ideal dusty gas flow for magnetic and non-magnetic case. The growth of the propagating waves for $\delta < 0$ is slowed down in the presence of the small solid dust particles in the medium of flow which is shown in Fig.4.2. Also, Fig.4.2 depicts that the parameter ϵ in dust free gas accelerates the growth of the propagating waves for $\delta < 0$. Thus, the growth rate of a compressive discontinuities in a dusty gas is lower than that of a dust-free gas. Also, in non-magnetic case, the expansive discontinuities decay later as compared to the magnetic case. The decay of the propagating waves for $\delta > 0$ and growth of the propagating waves for $\delta < 0$, respectively for non-ideal dusty gas flow in planar magnetic and non-magnetic case are shown in Fig.4.3 and Fig.4.4. It is observed that the non-ideal parameter b together with the mass fraction k_p enhances the flattening of expansive discontinuities and reduces the time for shock formation in both magnetic and non-magnetic case.

The decay of the propagating waves for $\delta > 0$ and growth of the propagating waves for $\delta < 0$, respectively for ideal dusty gas flow in non-planar (cylindrically symmetric) magnetic and non-magnetic case are shown in Fig.4.5 and Fig.4.6. Also, Fig.4.7 and Fig.4.8 respectively represents the decay of propagating waves for $\delta > 0$ and $\delta < 0$ non-ideal dusty non-planar ($m = 1$) flow for magnetic and non-magnetic case. A similar behavior can be seen from Fig.4.7 and Fig.4.8 for non-planar flow as in case of planar flow. A comparative analysis for expansive and compressive discontinuities in planar and cylindrically symmetric flows is shown by Fig.4.9 and Fig.4.10, respectively. From Fig.4.9, it is clear that the expansive discontinuities

decay more rapidly in the case of non-planar flow as compared to the planar flow in both dusty and non-dusty medium. Fig.4.10 shows that the compressive discontinuities grow later in the case of cylindrically symmetric flow as compared to the planar flow. Also, we observe that in the case of cylindrically symmetric flow, the shock formation is delayed whereas in case of planar flow, it forms earlier, i.e. the compressive discontinuities terminate into the shock wave earlier in case of planar flow as compared to the cylindrically symmetric flow.

4.7 Conclusion

In this chapter, the propagation of shock wave in one-dimensional van der Waals dusty magnetogasdynamic flow is studied. The impact of dust particles on the evolution of acceleration discontinuities in the presence of a magnetic field for planar and cylindrically symmetric flow is examined. Also, the condition for the shock formation has been derived and it is found that the compressive discontinuities terminate into the shock after a finite time and the expansive discontinuities smoother in infinite time. Effect of mass fraction of dust particles and the van der Waals parameter on the steepening or flattening of the waves for planar and cylindrically symmetric flows is studied. The presence of the dust particles is observed to decrease the decay rate of expansive discontinuities and reduces the chances of the shock formation. In the absence of the magnetic field and the van der Waals excluded volume, the results obtained in this chapter agrees with the results obtained in [91]. Also, we noticed that the non-ideal parameter b, together with a mass fraction of dust particles causes to increase the time for decay of expansive discontinuities and also enhance the growth process of compressive discontinuities for both magnetic and non-magnetic case. It is observed that in planar flow, the propagating waves for $\delta > 0$ decay later as

compared to the cylindrically symmetric flow. The propagating waves for $\delta < 0$ end up with the shock earlier in planar flow than the cylindrically symmetric flow. The entire study concluded that in both cases, planar and cylindrically symmetric flows, the decay rate of the propagating waves for $\delta > 0$ decreases, and also, the time for the shock formation increases due to an added effect of presence of dust particles in the medium.

****